IEEE Access
Multidisciplinary ⋮ Rapid Review ⋮ Open Access Journal

Received 7 June 2024, accepted 22 June 2024, date of publication 25 June 2024, date of current version 2 July 2024.

Digital Object Identifier 10.1109/ACCESS.2024.3419001

RESEARCH ARTICLE

Fuzzy Backstepping Control to Enhance Electric Power Steering System Performance

DUC NGOC NGUYEN AND TUAN ANH NGUYEN
Faculty of Mechanical Engineering, Thuyloi University, Hanoi 116705, Vietnam
Corresponding author: Tuan Anh Nguyen (anhngtu@tlu.edu.vn)

ABSTRACT The Electric Power Steering (EPS) system performs exceptionally well in ensuring safety and stability when steering. Although the robust Backstepping Control (BSC) technique is highly effective in controlling the system, it still has drawbacks regarding system errors and phase delays. A new combination called Fuzzy Backstepping Control (FBSC) is established in this work to eliminate the influence of error and phase difference phenomena, which is considered a new contribution to the paper. The input of the fuzzy algorithm is the systematic error and its derivative. At the same time, the fuzzy output is synthesized with a reference signal to become a new reference signal for the BSC technique. The stability of the control method is evaluated based on the Lyapunov criterion, while the system performance is evaluated according to the simulation process. According to the research findings, the value obtained from the proposed controller tends to closely follow the reference value with minor errors, and the phase delay phenomenon is almost completely eliminated. System performance is ensured under various simulation conditions, even when inputs (velocity and driver torque) change. Overall, the fuzzy backstepping control algorithm proposed in this work can maintain stability and improve the system's adaptability under different steering conditions.

INDEX TERMS Electric power steering, backstepping control, fuzzy control, steering column angle, steering motor angle.

NOMENCLATURE

ACO	Ant Colony Optimization.
ADRC	Active Disturbance Rejection Control.
BPNN	Backpropagation Neural Network.
BSC	Backstepping Control.
EHPS	Electrohydraulic Power Steering.
EPS	Electric Power Steering.
FBSC	Fuzzy Backstepping Control.
GA	Genetic Algorithm.
HPS	Hydraulic Power Steering.
LPV	Linear Parameter-Varying.
LQE	Linear Quadratic Estimation.
LQR	Linear Quadratic Regulator.
MSE	Mean Square Error.
PAS	Power-Assisted Steering.
PID	Proportional Integral Derivative.
RMS	Root Mean Square.
SMC	Sliding Mode Control.
WTAVER	Weighted Average.

The associate editor coordinating the review of this manuscript and approving it for publication was Ali Raza.

I. INTRODUCTION

A. POWER-ASSISTED STEERING SYSTEM

The Power-Assisted Steering (PAS) system was invented about 70 years ago by American companies [1]. This system is known by three names: Hydraulic Power Steering (HPS), Electric Power Steering (EPS), and Electrohydraulic Power Steering (EHPS). Most cars today are equipped with one of the above types of systems. Using the PAS system makes the steering process more accessible and more comfortable. The HPS system is often equipped with large vehicles [2]. Its structure is quite bulky, while its performance is not high. The EPS system offers many outstanding advantages compared to the conventional HPS system. Firstly, the EPS system's structure is compact, reducing its weight [3]. So, this system can be easily arranged in many locations (rack, steering column, or pinion types). Secondly, replacing HPS with EPS reduces energy consumption. In [4], Ramasany showed that the vehicle's energy consumption was improved by about 3%. Thirdly, the EPS system provides higher performance in ensuring vehicle stability and safety when steering at different speeds [5]. Additionally, the EPS system is more environmentally friendly than HPS because it does not use hydraulic oil. Finally, EPS operation is almost noiseless, while the HPS system often produces a strong vibration [6]. The EHPS system is a combination of EPS and HPS. However, this system still has the above disadvantages. EPS systems are commonly used on family vehicles, including mini-vans, pickups, sedans, SUVs, hatchbacks, and others [7]. Some large vehicles are often equipped with the EPS system with two independent electric motors to generate sufficient assisted torque [8].

B. LITERATURE REVIEW

The performance of the EPS system depends mainly on its control algorithm. If the system is considered linear, some traditional algorithms can be applied. A classical Proportional Integral Derivative (PID) controller was designed in [9] by Hassan et al. to control the C-EPS system model (column type). The parameters of this controller were calculated by a Genetic Algorithm (GA) to minimize the objective function. In [10], Hanifah et al. applied an Ant Colony Optimization (ACO) algorithm to tune parameters for the PID controller of the steering system, which was equipped with an electric vehicle. The target of this work was similar to [9], that is, to minimize the Mean Square Error (MSE) to reduce energy consumption. The results in [10] showed that assisted current decreased slightly (about 0.03 A) when replacing the classic PID controller with PID-ACO. A combination of PID and fuzzy techniques was shown by Cao and Zheng [11]. This algorithm was applied to an integrated dynamics model that combined the suspension and steering systems. In [12]. Li et al. applied the Backpropagation Neural Network (BPNN) technique to tune parameters for the PID controller of the EPS system. The structure of this algorithm included three layers: the input layer, the intermediate layer, and the output layer. Simulation results in [12] showed that the controlled signal tracked smoothly to the desired signal. The system's response speed was good. However, phase lag appeared when the vehicle steered at low speed. A phase-compensated fuzzy PI technique was shown in [13] by Zheng and Wei. They claimed that the current tracking effect was improved by 75.2% when applying this technique. A linear filter was fitted to the system to improve the delay margin [14]. Under the influence of external disturbances, the output results chattered when only the PID control technique was applied to control the system [15]. Simulation results in [16] showed that chattering and phase shift phenomena occurred strongly when applying the integrated PI-PID controller. An architecture of an adaptive network-based fuzzy inference system and PD was introduced in [17] by Ramos-Fernández et al. However, the tracking error was quite large, caused by two reasons: the training algorithm has not been optimally designed, and the training data has not been fully provided. The PID algorithm only applies to simple systems (one input and one output). The Linear Quadratic Regulator (LQR) technique suits systems with multiple inputs and outputs. In [18], Chitu et al. designed traditional LQR control for automotive EPS systems based on cost function minimization. To improve the performance of LQR, a state space observer was combined with the LQR technique to become a Linear Quadratic Estimation (LQE) [19]. It is not easy to evaluate the performance of these controllers because the simulation results in [18] and [19] are not fully mentioned. For systems with variable parameters, using the Linear Parameter-Varying (LPV) technique can be highly effective [20].

In reality, most systems are nonlinear or affine. Therefore, applying traditional control techniques (such as PID or LQR) will be ineffective. Lee et al. showed that the results obtained from simple controllers for linear systems are either non-convergent or continuously oscillating [21]. In [22], Zhao et al. compared the output results obtained from PID and H_∞ control. Simulation results in [22] showed that the step response obtained from H_∞ is closer to the reference value than PID. The calculations from [23] also showed that the PID controller had overshoot and phase shift problems compared to nonlinear robust controllers. A robust control method, Sliding Mode Control (SMC), has been applied to model the automotive EPS system. However, the chattering phenomenon occurred strongly when applying this technique [24]. In [25], Lee et al. designed an adaptive SMC algorithm for steering wheel torque tracking. The steering wheel angle value followed the reference value with an average error, but the steering wheel rate and acceleration were strongly affected by chattering. An improvement was shown in [26] by Lu et al. They designed a fuzzy algorithm to calibrate the SMC technique to minimize chattering effects. The Active Disturbance Rejection Control (ADRC) technique was applied to control the automotive EPS system to reduce the influence of external disturbances. This algorithm aimed to control the object so that it followed the steering wheel torque [27]. The simulation results in [27] showed that the angle error was quite small, while the angular speed error was relatively large. Another application of ADRC was performed by Ma et al. [28]. However, the improvement in results was not significant. In [29], Zheng and Wei compared ADRC, fuzzy PI, and classic PID. The performance of the ADRC algorithm was higher than the other two algorithms, but the output signal (motor current) was affected by chattering. Fu et al. presented an oscillation torque suppression control technique in [30]. However, signal interference still occurred, although this problem was significantly improved. In [31], Lee et al. designed a new controller based on combining two modules for steering torque tracking. The calculation results in [31] showed that the systematic error was relatively large. Backstepping Control (BSC) should replace the SMC algorithm to limit the effects of chattering and eliminate errors. An application of BSC to the EHPS system was presented in [32] by Shi et al. Compared to fuzzy PI, backstepping control provides superior performance. A combination of BSC and PI to control the EPS system was implemented by Nguyen and Nguyen [33]. The final control signal was synthesized from the two component signals. However, theoretical stability was evaluated based on only one technique instead of both. Nguyen presented an improvement of the BSC algorithm in [34]. To reduce phase shift, the input signal of the BSC technique was corrected by the PI technique. The parameters of the PI controller were tuned by the fuzzy algorithm with two inputs: driver torque and vehicle speed (k_p), driver torque and steering motor angle error (k_i).

Several intelligent control methods have also been applied to the EPS system. In [35], Li et al. designed a robust Takagi-Sugeno (T-S) fuzzy controller for system control. However, they did not specifically describe fuzzy rules or mention membership functions. Hung et al. designed a fuzzy neural network wavelet algorithm based on asymmetric membership functions [36]. Simulation results show that the angle tracking error could be up to 30.42° for the peak value and 7.19° for the average value. Robust fuzzy control was designed based on the two-layer performance presented by Fu et al. in [37]. In [38], You et al. introduced a neural approximation algorithm based on adaptive control for steering wheel torque tracking. The systematic error obtained from [38] was generally relatively large. In addition to fuzzy control, other intelligent control algorithms, such as neuroadaptive control and adaptive optimal control, help identify unknown dynamics and improve robustness. These algorithms are highly efficient and can be utilized to improve system quality [39], [40]. Some other control methods should be referenced in [41] and [42].

There are still some drawbacks from the above studies: 1) The power consumption of the controller is relatively large [10], [43]; 2) Signal noise and phase shift occur when applying traditional control algorithms (PID or LQR) to nonlinear systems [12], [15], [16], [23]. In addition, overshoot and non-convergence phenomena also negatively affect system quality [21], [23]; 3) The system error is relatively large, even when applying robust control techniques for nonlinear systems or intelligent control algorithms [17], [25], [27], [31], [36], [38]; 4) Chattering phenomenon occurs in output signals when using SMC or ADRC techniques [24], [25], [27], [29]; 5) Road reaction torque is ignored during the calculation or is assumed to be known in advance or calculated in a simple way [30], [31], [38], [44], [45], [46]; 6) External disturbances are not mentioned in most previous publications. In this paper, we propose to design a robust nonlinear algorithm to solve the above disadvantages. This algorithm combines the BSC and fuzzy methods, called Fuzzy Backstepping Control (FBSC). This combination is highly effective in eliminating phase shift (2nd issue), reducing systematic errors (3rd issue), limiting the influence of chattering (4th issue) and improving energy consumption performance (1st issue). The 5th issue is solved by applying a single-track dynamics model to calculate road reaction torque. Finally, the influence of external disturbances is fully considered instead of ignored, as in previous studies.

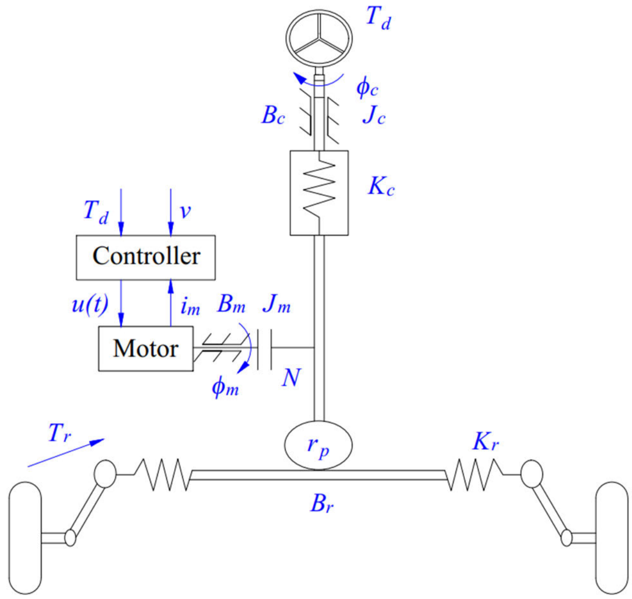

FIGURE 1. EPS system model.

Overall, the paper makes three main contributions to solving existing issues. Firstly, the proposed algorithm can eliminate errors and phase shift phenomena. Secondly, this algorithm can help reduce the adverse effects of chattering. Thirdly, applying this technique will lead to an improvement in the system's energy consumption. Furthermore, the influence of dynamic factors and disturbances is fully considered when investigating the vehicle's steering process. These are considered outstanding contributions to the paper that differentiate it from other publications.

The paper's structure consists of four sections. The first section (introduction) mentions the literature review and work motivation. The system model, including the EPS and control models, is presented in the second section (mathematical model). The following section (simulation and result) gives numerical simulation results and discussion. The final section (conclusion) addresses the proposed algorithm's limitations and future development directions.

II. MATHEMATICAL MODEL

A. EPS MODEL

Figure 1 describes the structure of a C-EPS system equipped on a car. Driver torque from the driver is transmitted directly to the steering wheel. It is then transmitted to a steering column and a steering mechanism. The steering mechanism of this system includes a rack and a pinion. The steering column is assisted by a pair of gears driven by an electric motor. The assisted motor is controlled by an electric control unit based on the established control algorithm.

The relationship between the steering column angle (ϕ_c) and steering motor angle (ϕ_m) is described by equation (1). The dependence of the steering motor angle (ϕ_m) on motor current (i_m) is illustrated by equation (2). The relationship between the steering column angle, steering motor angle, and motor current is mentioned in (3).

$$J_c\ddot{\phi}_c + B_c\dot{\phi}_c + K_c\phi_c = \frac{K_c}{N}\phi_m + T_d \tag{1}$$

$$K_t\dot{\phi}_m + L_m\dot{i}_m + R_m i_m = u(t) \tag{2}$$

$$\frac{K_c}{N}\phi_c + K_t i_m - \frac{T_r}{N} = J_{eq}\ddot{\phi}_m + B_{eq}\dot{\phi}_m + \frac{K_c + K_r r_p^2}{N^2}\phi_m \tag{3}$$

The equivalent damping coefficient (B_{eq}) and equivalent moment of inertia (J_{eq}) are calculated according to (4) and (5), respectively, where J_c and J_m are the inertia moment of the steering column and steering motor, respectively; B_c, B_m, and B_r are steering column damping, steering motor damping, and rack damping, respectively; N is motor ratio, K_t is motor torque coefficient, K_c is torsional stiffness of the steering column, T_d is driver torque, M_r is rack mass, r_p is pinion radius, R_m is motor resistance, and L_m is motor inductance.

$$B_{eq} = B_m + \frac{r_p^2}{N^2}B_r \tag{4}$$

$$J_{eq} = J_m + \frac{r_p^2}{N^2}M_r \tag{5}$$

System disturbances (T_r) include two components: internal noise (T_{id}) and external noise (T_{ed}). External travel factors, such as road surface bumps, crosswinds, weather conditions, and others cause external disturbances. In contrast, internal disturbances are the result of steering, also known as steering resistance moment. Equations (6) and (7) provide information on determining internal and system disturbances, where l_n is knuckle arm length; l_c is the caster trail; F_y is lateral tire force; γ_k and γ_c are kingpin and caster angle, respectively.

$$T_{id} \approx r_p l_c \frac{cos^2(\gamma_k)\,cos^2(\gamma_c)}{l_n}F_{yf} \tag{6}$$

$$T_r = T_{id} + T_{ed} \tag{7}$$

The lateral force at the wheel is calculated by the tire model. The Pacejka tire model accurately calculates aggressive steering conditions (vehicle steering at very high speed with a large steering angle) [47]. However, calculating the Pacejka model is complicated and requires many experimental parameters. Assuming the tire deforms in the linear domain (*), a linear tire model can be applied with acceptable accuracy. Equations (8) and (9) provide information on determining the value of the lateral force at tires when steering (f is the symbol for the front, and r is the symbol for the rear).

$$F_{yf} = -C_{\alpha f}\alpha_f \tag{8}$$

$$F_{yr} = -C_{\alpha r}\alpha_r \tag{9}$$

The tire's cornering stiffness (C_α) is a constant, while the tire's slip angle (α) changes over time. Its variation depends on yaw angle (ψ), vehicle speed (v), and steering angle (δ). This relationship is described by equations (10) and (11).

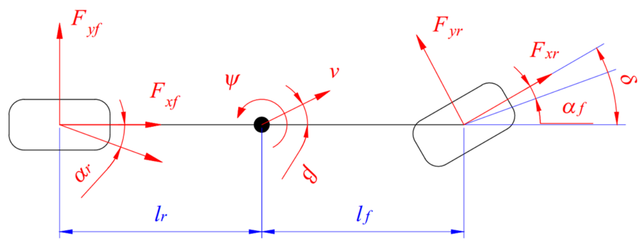

FIGURE 2. Vehicle model.

$$\alpha_f = \frac{v_y + l_f\dot{\psi}}{v_x} - \delta \tag{10}$$

$$\alpha_r = \frac{v_y - l_r\dot{\psi}}{v_x} \tag{11}$$

A single-track dynamics model is illustrated in Figure 2. The motion of the car when steering is described by equations (12), (13), and (14), where J_z is the moment of inertia of the vehicle; l_f and l_r are the vehicle's dimensions (Figure 2); m is the mass of the vehicle.

$$m\left(\dot{v}_x - \dot{\psi}v_y\right) = F_{xf}cos\delta + F_{xr} - F_{yf}sin\delta \tag{12}$$

$$m\left(\dot{v}_y + \dot{\psi}v_x\right) = F_{yf}cos\delta + F_{yr} + F_{xf}sin\delta \tag{13}$$

$$J_z\ddot{\psi} = l_f\left(F_{xf}sin\delta + F_{yf}cos\delta\right) - l_rF_{yr} \tag{14}$$

To satisfy condition (*), the steering angle must be slightly sufficient, i.e. $sin\delta \approx 0$ and $cos\delta \approx 1$. As a result, equation (13) becomes (15), and equation (14) becomes (16). One thing to note is that equation (12) will be eliminated when steering at a steady speed ($v = $ const).

$$m\left(\dot{v}_y + \dot{\psi}v_x\right) = F_{yf} + F_{yr} \tag{15}$$

$$J_z\ddot{\psi} = l_fF_{yf} - l_rF_{yr} \tag{16}$$

According to equations (17) and (18), the longitudinal velocity (v_x) and lateral velocity (v_y) are determined based on the heading angle (β).

$$v_x = v\cos\beta \tag{17}$$

$$v_y = v\sin\beta \tag{18}$$

According to condition (*), the heading angle is slight. If the vehicle moves at a constant speed, the relationship between v_y and v_x can be described as (19).

$$\dot{v}_y \approx v_x\dot{\beta} \tag{19}$$

Combining equations (8), (9), (10), (11), (15), (16), and (19), we get (20). Equation (20) describes the vehicle's motion when steering.

$$\begin{bmatrix}\dot{\beta}\\ \ddot{\psi}\end{bmatrix} = \boldsymbol{A}\begin{bmatrix}\beta\\ \dot{\psi}\end{bmatrix} + \boldsymbol{B}[\delta] \tag{20}$$

where

$$\boldsymbol{A}=\begin{bmatrix}-\dfrac{C_{\alpha f}+C_{\alpha r}}{mv_x} & \dfrac{-l_fC_{\alpha f}+l_rC_{\alpha r}}{mv_x^2}-1\\ -\dfrac{l_fC_{\alpha f}-l_rC_{\alpha r}}{J_z} & -\dfrac{l_f^2C_{\alpha f}+l_r^2C_{\alpha r}}{J_z\psi}\end{bmatrix}$$

$$\boldsymbol{B}=\begin{bmatrix}\dfrac{C_{\alpha f}}{mv_x}\\ \dfrac{l_fC_{\alpha f}}{J_z}\end{bmatrix}$$

B. CONTROL MODEL

Set the state variables according to (21).

$$\begin{bmatrix}x_1 & x_2 & x_3 & x_4 & x_5\end{bmatrix}^T=\begin{bmatrix}\phi_c\\ \dot{\phi}_c\\ \phi_m\\ \dot{\phi}_m\\ i_m\end{bmatrix} \tag{21}$$

We get equations from (22) to (26) by taking the derivative of the state variables x_i.

$$\dot{x}_1=x_2 \tag{22}$$
$$\dot{x}_2=-\frac{K_c}{J_c}x_1-\frac{B_c}{J_c}x_2+\frac{K_c}{J_cN}x_3+\frac{T_d}{J_c} \tag{23}$$
$$\dot{x}_3=x_4 \tag{24}$$
$$\dot{x}_4=\frac{K_c}{J_{eq}N}x_1-\frac{K_c+K_rr_p^2}{J_{eq}N^2}x_3-\frac{B_{eq}}{J_{eq}}x_4+\frac{K_t}{J_{eq}}x_5-\frac{T_r}{J_{eq}N} \tag{25}$$
$$\dot{x}_5=-\frac{K_t}{L_m}x_4-\frac{R_m}{L_m}x_5+\frac{1}{L_m}u\left(t\right) \tag{26}$$

The object to be controlled is the steering motor angle (x_3). In this work, we propose the use of the robust backstepping control (BSC) technique to control this object. The error between the actual value (x_3) and the reference value (x_{3_ref}) is denoted as e_1, according to (27). Taking the derivative of (27), we get (28).

$$e_1=x_3-x_{3\_ref} \tag{27}$$
$$\dot{e}_1=\dot{x}_3-\dot{x}_{3\_ref}=x_4-\dot{x}_{3\_ref} \tag{28}$$

Equations (29) and (30) denote the virtual errors of the system as e_2 and e_3. The first virtual control variable of the system (λ_1) is selected according to (31) and the second virtual control variable (λ_2) is selected according to (32), where K_1 is the proportionality constant between x_5 and x_{3_ref} and d_1 is the specific constant.

$$e_2=x_4-\lambda_1 \tag{29}$$
$$e_3=x_5-\lambda_2 \tag{30}$$
$$\lambda_1=\dot{x}_{3\_ref}-d_1e_1 \tag{31}$$
$$\lambda_2=K_1x_{3\_ref} \tag{32}$$

Combining equations (28), (29), and (31), we get (33). According to (33), the value of e_2 will approach the derivative of e_1 if e_1 approaches zero. This proves that the first virtual control variable (λ_1) is chosen appropriately.

$$\begin{aligned}e_2&=x_4-\left(\dot{x}_{3\_ref}-d_1e_1\right)=x_4+\left(\dot{e}_1-x_4\right)+d_1e_1\\&=\dot{e}_1+d_1e_1\xrightarrow{e_1\to 0}\dot{e}_1\end{aligned} \tag{33}$$

Substituting equations (29) and (31) into (28), we get (34).

$$\dot{e}_1=\left(e_2+\lambda_1\right)-\left(\lambda_1+d_1e_1\right)=e_2-d_1e_1 \tag{34}$$

Equations (35) and (36) are obtained by differentiating (29) and (31), respectively.

$$\dot{e}_2=\dot{x}_4-\dot{\lambda}_1 \tag{35}$$
$$\dot{\lambda}_1=\ddot{x}_{3\_ref}-d_1\dot{e}_1 \tag{36}$$

Substituting equations (34) and (36) into (35), we get (37). Equation (38) is established based on the combination of (25) and (37).

$$\dot{e}_2=\dot{x}_4-\left(\ddot{x}_{3\_ref}-d_1\dot{e}_1\right)=\dot{x}_4-\ddot{x}_{3\_ref}+d_1\left(e_2-d_1e_1\right) \tag{37}$$

$$\dot{e}_2=\frac{K_c}{J_{eq}N}x_1-\frac{K_c+K_rr_p^2}{J_{eq}N^2}x_3-\frac{B_{eq}}{J_{eq}}x_4+\frac{K_t}{J_{eq}}x_5-\frac{T_r}{J_{eq}N}+d_1e_2-d_1^2e_1-\ddot{x}_{3\_ref} \tag{38}$$

Substituting equations (29) and (31) into (38), we get (39), where the symbol d_2 is described by (40).

$$\begin{aligned}\dot{e}_2=&\frac{K_c}{J_{eq}N}x_1+\left(d_1\frac{B_{eq}}{J_{eq}}-\frac{K_c+K_rr_p^2}{J_{eq}N^2}\right)x_3+\frac{K_t}{J_{eq}}x_5\\&-\left(d_1\frac{B_{eq}}{J_{eq}}x_{3\_ref}+\frac{B_{eq}}{J_{eq}}\dot{x}_{3\_ref}+\ddot{x}_{3\_ref}\right)\\&-\left(\frac{T_r}{J_{eq}N}+d_1^2e_1\right)-d_2e_2=f_1\left(x\right)-d_2e_2\end{aligned} \tag{39}$$

$$d_2=\frac{B_{eq}}{J_{eq}}-d_1 \tag{40}$$

Taking the derivative of (30), we get (41). Substituting equations (26) and (32) into (41), we obtain (42).

$$\dot{e}_3=\dot{x}_5-\dot{\lambda}_2 \tag{41}$$

$$\begin{aligned}\dot{e}_3=&-\frac{K_t}{L_m}x_4-\frac{K_1R_m}{L_m}x_{3\_ref}-K_1\dot{x}_{3\_ref}\\&-\frac{R_m}{L_m}e_3+\frac{1}{L_m}u\left(t\right)=f_2\left(x\right)+\frac{1}{L_m}u\left(t\right)-\frac{R_m}{L_m}e_3\end{aligned} \tag{42}$$

1) STABILITY PROOFS

A Lyapunov control function $V(x)$ is chosen according to (43). Taking the derivative of $V(x)$, we get (44).

$$V\left(x\right)=\frac{1}{2}e_1^2+\frac{1}{2}e_2^2+\frac{1}{2}e_3^2 \tag{43}$$
$$\dot{V}\left(x\right)=e_1\dot{e}_1+e_2\dot{e}_2+e_3\dot{e}_3 \tag{44}$$

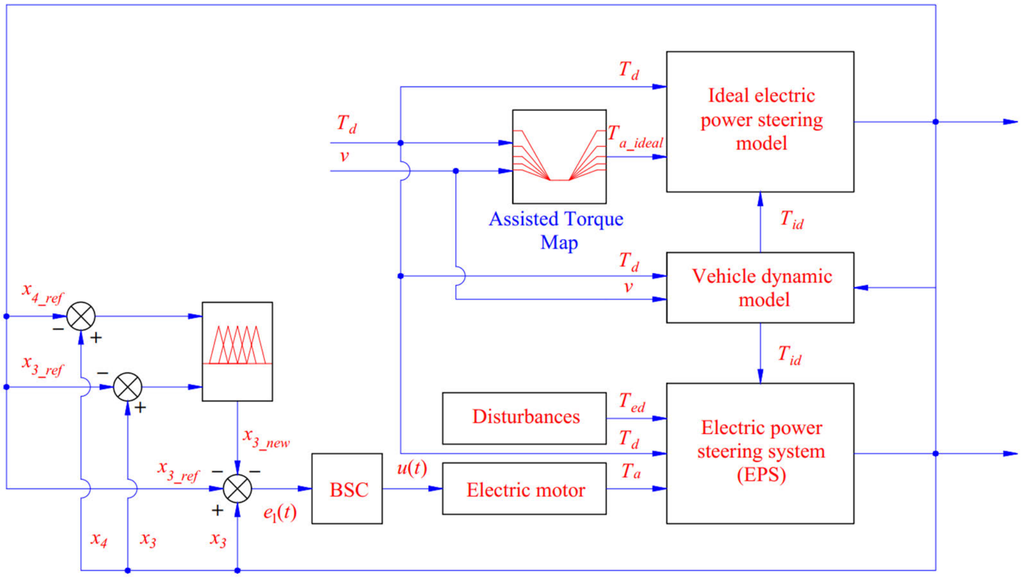

FIGURE 3. Control scheme.

Substituting equations (34), (39), and (42) into (44), we get (45).

$$\dot{V}(x) = \left(-d_1e_1^2 - d_2e_2^2 - d_3e_3^2\right) + \left(e_1e_2 + e_2f_1(x) + e_3f_2(x) + \frac{e_3}{L_m}u(t)\right) \tag{45}$$

The control signal $u(t)$ is selected according to (46) with the symbol d_3 described as (47).

$$u(t) = -L_m\left[\frac{e_2(f_1(x) + e_1)}{e_3} + f_2(x)\right] \tag{46}$$

$$d_3 = \frac{R_m}{L_m} \tag{47}$$

Substituting equation (46) into (45), we obtain (48).

$$\dot{V}(x) = -d_1e_1^2 - d_2e_2^2 - d_3e_3^2 \tag{48}$$

$$0 < d_1 < \frac{B_{eq}}{J_{eq}} \tag{49}$$

According to (43) and (48), the proposed Lyapunov control function is positive definite, and its derivative is negative definite $\forall x \neq 0$ (if and only if d_1 satisfies condition (49)). Therefore, the controller designed for this work is considered stable.

According to (46), determining the control signal $u(t)$ when e_3 is zero is extremely difficult. In [34], Nguyen proposed a solution to simplify this calculation process. However, using an approximate calculation model causes systematic errors to increase (the signal is phase delayed or phase advanced). To solve this problem, we propose to design a fuzzy algorithm to correct the value of the reference signal, i.e., x_{3_ref} becomes $x_{3\_ref\_new}$ (Figure 3). The new reference signal ($x_{3\_ref\_new}$) is determined according to (50).

$$x_{3\_ref\_new} = x_{3\_ref} + x_{3\_new} \tag{50}$$

x_{3_new} is the fuzzy controller's output signal. This controller has two inputs: a steering motor rate error (1st input) and a steering motor angle error (2nd input). The membership functions of the fuzzy controller are depicted in Figure 4. The first input is defined in terms of Gaussian functions (51), while the second input is computed in terms of triangular (52) and trapezoidal (53) functions.

$$f_1(\dot{e}_1; \sigma, c) = e^{\frac{-(\dot{e}_1 - c)^2}{2\sigma^2}} \tag{51}$$

$$f_2(e_1; a, b, c) = \max\left(\min\left(\frac{e_1 - a}{b - a}, \frac{c - e_1}{c - b}\right), 0\right) \tag{52}$$

$$f_2(e_1; a, b, c, d) = \max\left(\min\left(\frac{e_1 - a}{b - a}, 1, \frac{d - e_1}{d - c}\right), 0\right) \tag{53}$$

where a, b, c, d, and σ are coefficients of membership functions.

The defuzzification process is performed using the Weighted Average (WTAVER) method. Fuzzy rules are proposed in Table 1, including Large Negative (LNE), Negative (NEG), Neutral (NEU), Positive (POS), and Large Positive (LPO).

The fuzzy surface describes the dependence of the output signal on two input signals in Figure 5. This fuzzy surface is formed based on the fuzzy rules listed in Table 1.

The choice of parameters for the controller is essential for real applications. In this work, the coefficients d_1, d_2, and d_3 are chosen according to (49), (40), and (47) respectively. The system's quality depends mainly on the choice of membership functions and fuzzy rules. The response-ability needs to be high regarding the steering motor angle (controlled

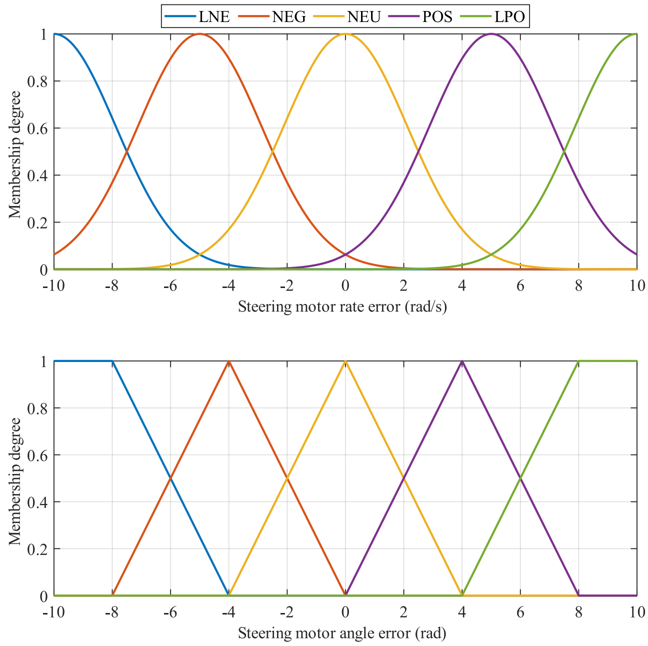

FIGURE 4. Membership functions.

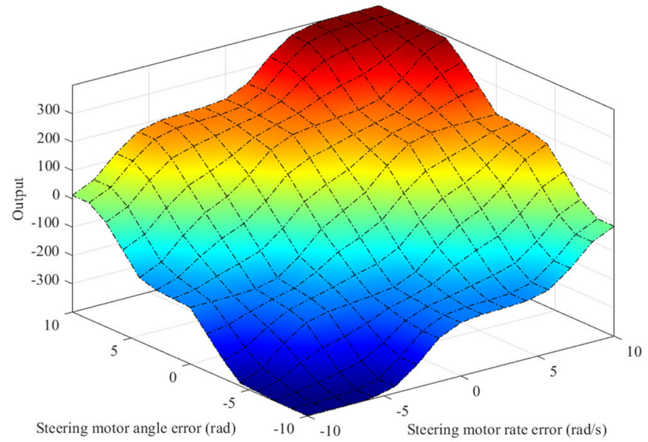

FIGURE 5. Fuzzy surface.

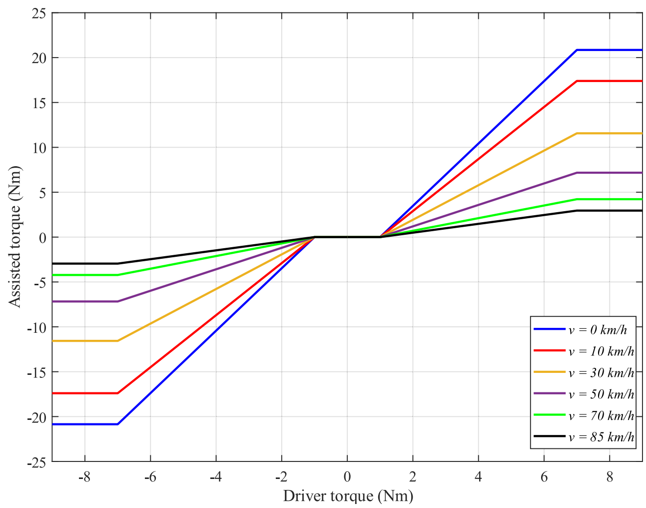

FIGURE 6. Ideal assisted torque map.

TABLE 1. Fuzzy rules.

1st input	2nd input	Output	1st input	2nd input	Output
LNE	LNE	LNE	NEU	POS	POS
LNE	NEG	LNE	NEU	LPO	POS
LNE	NEU	NEG	POS	LNE	NEG
LNE	POS	NEG	POS	NEG	NEU
LNE	LPO	NEU	POS	NEU	POS
NEG	LNE	LNE	POS	POS	POS
NEG	NEG	NEG	POS	LPO	LPO
NEG	NEU	NEG	LPO	LNE	NEU
NEG	POS	NEU	LPO	NEG	POS
NEG	LPO	POS	LPO	NEU	POS
NEU	LNE	NEG	LPO	POS	LPO
NEU	NEG	NEG	LPO	LPO	LPO
NEU	NEU	NEU			

object). Therefore, triangular functions are a suitable choice. To avoid oversensitivity in steering motor rate, triangular functions should be replaced with Gaussian functions. Their error ranges are selected according to experience gained from previous simulations. The proposed fuzzy law is based on ensuring response speed and avoiding simultaneous overshoot.

The reference signal x_{3_ref} is taken from the ideal model. The ideal model is supported by ideal assisted torque ($T_a = T_{a\_ideal}$), as shown in Figure 6.

Looking at Figure 6 more closely, one can see that the assisted motor will not operate ($T_{a\_ideal} = 0$) when the driver torque input is too tiny ($T_d < T_{d\_max}$). If the driver torque is large enough ($T_{d\_max} \geq T_d \geq T_{d\_min}$), the ideal assisted torque will increase linearly with the driver torque. Once the driver torque exceeds its limit ($T_d > T_{d\_max}$), the ideal assisted torque will reach saturation ($T_{a\_ideal} = T_{a\_max}$). The change in velocity has a significant influence on assisted torque. The assistance performance is excellent when the vehicle steers at a low speed and vice versa.

$$T_{a\_ideal} = \begin{cases} 0 & 0 \leq T_d < T_{d\_min} \\ \left(a_1 v^2 + a_2 v + a_3\right)\left(T_d - T_{d\_min}\right) & T_{d\_min} \leq T_d < T_{d\_max} \\ T_{a\_max} & T_d > T_{d\_max} \end{cases} \tag{54}$$

The relationship between ideal assisted torque, driver torque, and vehicle speed is described according to (54), where empirical coefficients are a_1, a_2, and a_3. The numerical simulation process will be conducted in the next section of this paper.

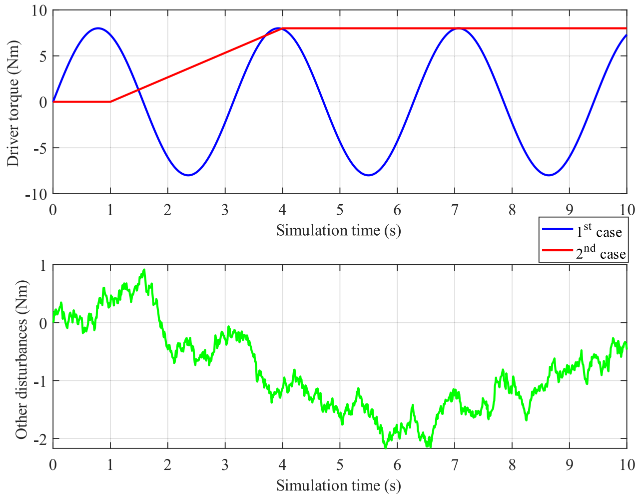

FIGURE 7. Simulation inputs.

TABLE 2. Technical parameters.

Symbol	Unit	Value	Symbol	Unit	Value
J_c	kgm^2	0.06	K_c	Nm/rad	126
J_m	kgm^2	0.0004	M_r	kg	31.5
B_c	Nms/rad	0.065	r_p	m	0.007
B_m	Nms/rad	0.0044	R_m	Ω	0.41
B_r	Ns/m	3630	L_m	H	0.007
N	-	17	l_c	m	0.032
K_t	Nm/A	0.058	l_n	m	0.31
$C_{\alpha f}$	N/rad	43500	γ_k	°	10
$C_{\alpha r}$	N/rad	43500	γ_c	°	5
l_f	m	1.11	m	kg	1650
l_r	m	1.69	J_z	kgm^2	3490

III. SIMULATION AND RESULT

A. SIMULATION CONDITION

The performance of the proposed controller is evaluated by simulation. The change in speed and driver torque is the input to the simulation problem. According to the first subplot in Figure 7, two types of torque drivers are used in this work: sine wave steering (the first case) and J-turn steering (the second case). The vehicle's moving speed is investigated at $v_1 = 20$ km/h and $v_2 = 70$ km/h. The effects of external disturbances (T_{ed}) are depicted in the remaining subplot in Figure 7. The outputs are depicted by the subplots in Figures 8, 9, 10, and 11, including steering column angle (the first subplot), steering column rate (the second subplot), steering motor angle (the third subplot), steering motor rate (the fourth subplot), motor current (the fifth subplot), and assisted torque (the final subplot).

The technical parameters used for the simulation are referenced in Table 2.

B. RESULT AND DISCUSSION

The simulation results are evaluated in two cases corresponding to two types of driver torque, as presented above.

1) THE FIRST CASE

Sine wave steering is used for the first case (Figure 7), while J-turn steering is applied for the second case. In each case, the vehicle's speed when steering is investigated at two different thresholds.

$v_1 = 20$ km/h: The changes in simulation outputs when steering at speed v_1 are depicted in Figure 8. According to the first subplot, the steering column angle changes based on the sinusoidal rule, corresponding to the driver torque input. If the EPS system is controlled by the BSC algorithm, the received output signal will be phase-delayed compared to the reference signal. As a result, the maximum steering column angle error obtained from this controller is 2.550 rad. Furthermore, the Root Mean Square (RMS) error and mean error are 1.377 rad and 0.226 rad, respectively. In general, the error caused by the backstepping controller when steering at speed v_1 is small. Compared to BSC, the values obtained from the FBSC algorithm tend to follow the reference signal better. According to simulation results, the maximum error of the steering column angle obtained from the proposed algorithm (FBSC) is only 0.064 rad. The RMS and mean errors obtained from the FBSC controller are extremely small, only 0.039 rad and 0.002 rad, respectively. Regarding the steering column rate, external disturbances cause the output signal to fluctuate slightly instead of being a smooth curve like the steering column angle. Simulation results show that the maximum error of BSC is up to 4.356 rad/s, 39.24 times higher than that of FBSC. Under this condition, the RMS error and mean error of the single backstepping controller are also relatively high (2.460 rad/s and 0.204 rad/s, respectively), while the error obtained from the fuzzy backstepping controller is much lower, only about 0.076 rad/s and 0.005 rad/s. Phase lag does not occur when the system is controlled by the FBSC technique, which is proposed in this work.

The steering motor angle is the controlled object, so investigating the change of this state variable is necessary. The third and fourth subplots in Figure 8 show the steering motor angle and steering motor rate change over time. Looking at Figure 8 more closely, we can see that the changing trend of the steering motor angle is similar to that of the steering column angle. However, the steering motor angle has a much greater value than the steering column angle. The same goes for steering motor rate and steering column rate. According to the calculation results, the maximum error, RMS error, and average error of the steering motor angle obtained from the BSC controller can be up to 43.298 rad, 23.377 rad, and 3.834 rad, respectively. The above numbers are much larger than the values obtained from the FBSC controller (1.076 rad, 0.659 rad, and 0.033 rad). When using the BSC technique, phase lag occurs for the controlled object (x_3) and its derivative (x_4).

The fifth subplot in Figure 8 describes the change in motor current when steering at speed $v_1 = 20$ km/h. According to this description, the motor current value obtained from the fuzzy backstepping controller always closely follows the reference value with a small error. Simulation results show that their RMS error is only 1.100 A, while the mean error

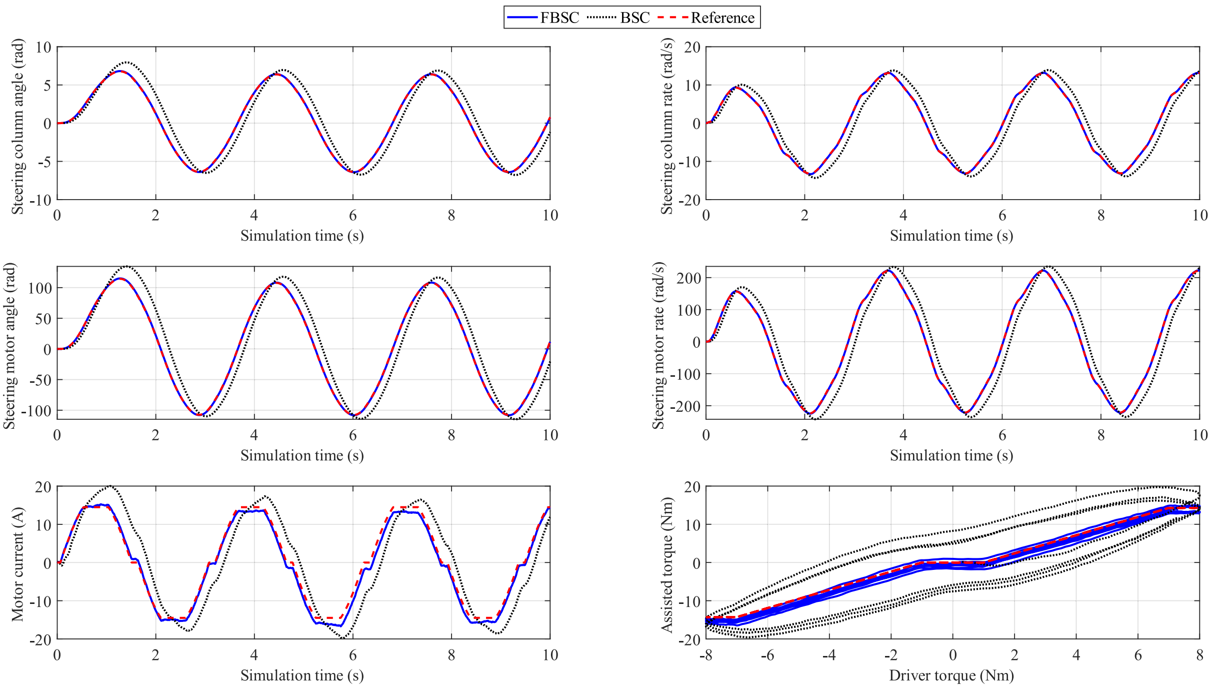

FIGURE 8. **Simulation results (v_1, sine wave steering).**

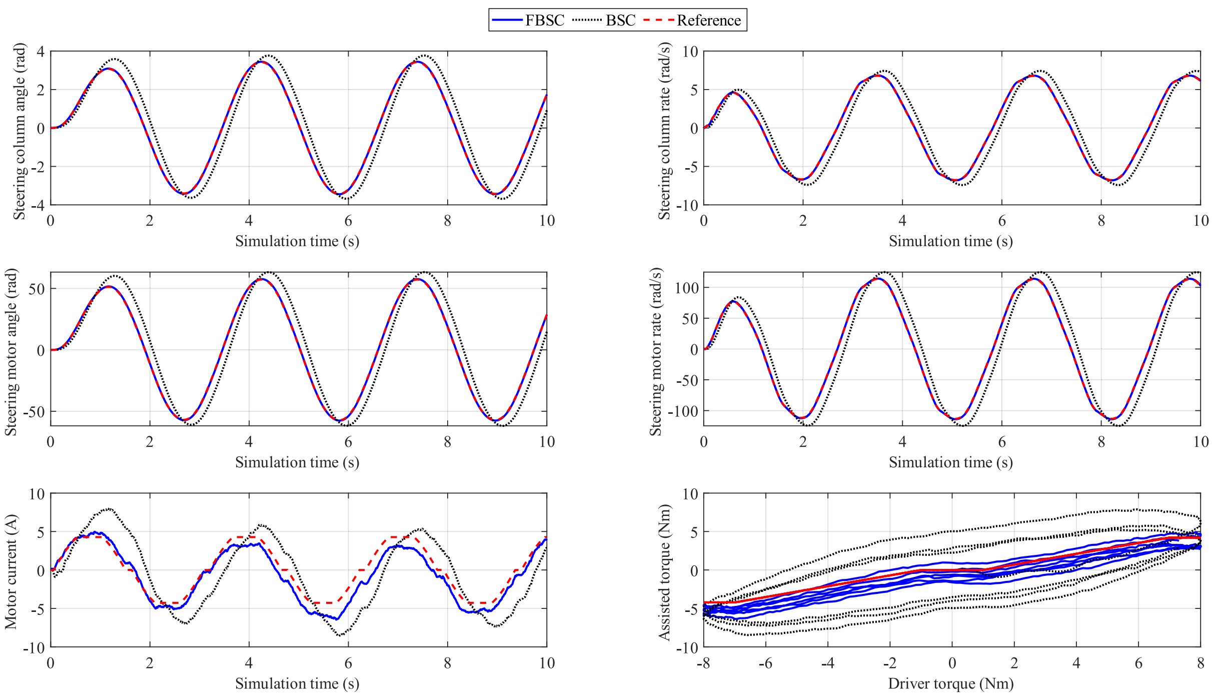

FIGURE 9. **Simulation results (v_2, sine wave steering).**

does not exceed 0.777 A. These errors increase when the conventional backstepping controller controls the EPS system (5.370 A and 4.073 A) instead of FBSC. This shows that the system energy consumption is improved when the BSC controller is replaced by FBSC.

The last subplot in Figure 8 depicts the relationship between driver and assisted torque. When $T_d < T_{d\_min}$, the assisted motor does not operate, causing $T_a = 0$. If T_d exceeds T_{d_min}, assisted torque will increase linearly with driver torque, and it will reach saturation when $T_d = T_{d\_max}$. This change perfectly agrees with the ideal characteristic curve depicted in Figure 3. Compared with conventional BSC, the assisted torque obtained from FBSC follows the reference value better with insignificant error.

$v_2 = 70$ *km/h:* According to the description in Figure 3, the steering assistance characteristic curve will change as the speed changes. Therefore, it is necessary to investigate the controller's performance at different speeds. The results in Figure 9 show that the state variables change when steering at speed $v_2 = 70$ km/h.

Looking at this figure more closely, the output values tend to decrease as the velocity increases. This is caused by a decrease in assisted torque and an increase in road reaction torque. According to the simulation results, the maximum error of the steering column angle can be up to 1.150 rad, while its RMS error and mean error are 0.725 rad and 0.056 rad, respectively. These values are achieved if and only if the EPS system is controlled by the conventional BSC algorithm. When applying this technique to control the system, a phase delay occurs. A significant improvement is seen in the results for the FBSC controller. According to the simulation results, the maximum error of the steering column angle is only 0.035 rad, and the RMS error is 0.022 rad, much lower than the results obtained from the single backstepping controller. After the results are rounded, the system mean error is considered to be approximately zero (FBSC). The phase difference phenomenon is completely eliminated when the FBSC technique is applied to replace conventional BSC. Compared with condition v_1, the systematic error (steering column rate) obtained in condition v_2 is smaller. These results are shown in Table 3.

The change of the controlled object (x_3) and its derivative (x_4) are shown in the third and fourth subplots of Figure 9. It is easy to see that the output values tend to decrease as velocity increases. As a result, the systematic error also decreased sharply. Simulation results show that the steering motor angle's RMS and average errors are only 0.373 rad and 0.003 rad, respectively. These data are achieved when the EPS system is controlled by the fuzzy backstepping algorithm proposed in this work.

The robust backstepping control technique ensures that system errors are stable. Under condition v_2, the average motor current error is relatively small, only 0.764 A for FBSC and 2.589 A for BSC. The system's energy consumption efficiency is improved when the BSC controller is replaced with the FBSC. The final subplot in Figure 9 shows the dependence of assisted torque on driver torque. Compared to condition v_1, the value of assisted torque in condition v_2 is strongly reduced. This is entirely consistent with the initially set rules (Figure 3).

$v_3 = 90$ *km/h:* The output changes are described in Figure 10 when steering at very high speed ($v_3 = 90$ km/h). Similar to v_2, the output value decreases as velocity increases. In this condition, the assisted power performance is not high. This helps improve stability and avoid vehicle rollover. The simulation values obtained under this condition are illustrated in Table 3. In general, the system error is inconsiderable if and only if the system is controlled by the algorithm proposed in this work (FBSC).

2) THE SECOND CASE

The second case refers to the J-turn steering style, often applied in practice when steering (Figure 7).

$v_1 = 20$ *km/h:* The steering assistance performance of the EPS system is high when the vehicle steers at low speed ($v_1 =$ 20 km/h). According to the description of the subplots in Figure 11, the results obtained from the BSC algorithm cannot follow the reference value. The error between the results is substantial. Simulation results show that the maximum error, RMS error, and average error of the steering column angle obtained from the single backstepping controller can be up to 4.578 rad, 2.505 rad, and 1.609 rad, respectively. These values are much higher than the errors obtained from the FBSC algorithm (0.065 rad, 0.041 rad, and 0.027 rad, respectively). The values obtained from the FBSC algorithm tend to track the reference value with negligible error for both the steering column angle and steering column rate. This is true for the steering motor angle (the controlled object) and the steering motor rate. A significant difference in value is seen when the EPS system is controlled only by the conventional BSC algorithm.

The motor current signal fluctuates under the influence of external disturbances (Figure 11). The fuzzy backstepping algorithm excels at controlling systematic errors, ensuring that the output signal follows the reference signal with minimal error. The simulation results show that the RMS and average errors of motor current obtained from the FBSC algorithm are only 0.835 A and 0.415 A, respectively. Compared to the BSC algorithm, the error of motor current obtained from FBSC is only 13.53% and 9.93%, respectively. According to the last subplot in Figure 10, the assisted torque obtained from the FBSC algorithm tends to track the reference value closely. However, the system error is significant when the EPS system is controlled by only the single BSC technique.

$v_2 = 70$ *km/h:* The results of the final investigation ($v_2 = 70$ km/h) are depicted in Figure 12. The output results show a sharp decline as the velocity increases from $v_1 = 20$ km/h to $v_2 = 70$ km/h. When the EPS system is controlled by the BSC algorithm, the system error is extremely large (for all five state variables). This can be solved by replacing the single BSC technique with the FBSC technique proposed in this work. According to research findings, the output values obtained from the fuzzy backstepping controller always closely match the desired value with tiny errors. The motor current signal fluctuates under the influence of external disturbances, but the RMS error and average error remain at an acceptable level.

$v_2 = 90$ *km/h:* Figure 13 provides information about the output values when steering at speed v_3. Compared with the above two conditions, the results obtained in this condition are minor. This is due to a decrease in assisted power

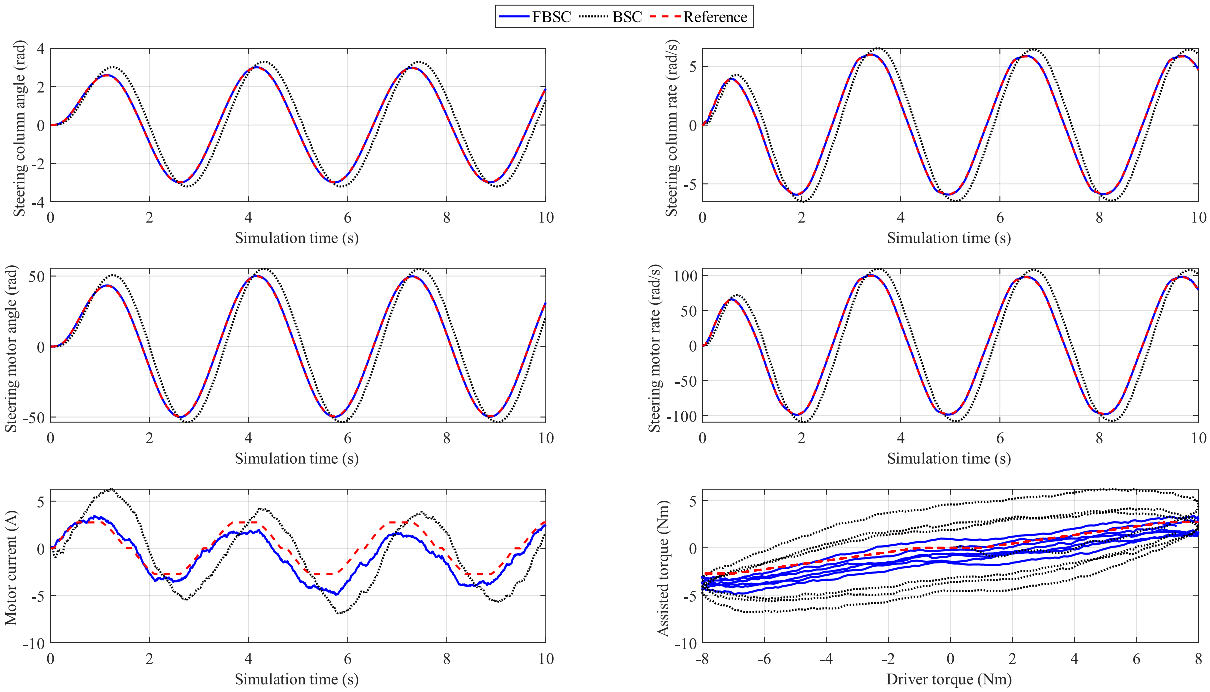

FIGURE 10. Simulation results (v_3, sine wave steering).

TABLE 3. Simulation results (1st case).

v_1 = 20 km/h	FBSC			BSC			Improvement (%)	
	Max	RMS	Mean	Max	RMS	Mean	RMS	Mean
Steering column angle error (rad)	0.064	0.039	0.002	2.550	1.377	0.226	97.168	99.115
Steering column rate error (rad/s)	0.111	0.076	0.005	4.356	2.640	0.204	97.121	97.549
Steering motor angle error (rad)	1.076	0.659	0.033	43.298	23.377	3.834	97.181	99.139
Steering motor rate error (rad/s)	1.869	1.282	0.091	73.908	44.777	3.467	97.137	97.375
Motor current error (A)	2.399	1.100	0.777	10.058	5.370	4.073	79.516	80.923
v_2 = 70 km/h	FBSC			BSC			Improvement (%)	
	Max	RMS	Mean	Max	RMS	Mean	RMS	Mean
Steering column angle error (rad)	0.035	0.022	≈ 0	1.150	0.725	0.056	96.966	100.000
Steering column rate error (rad/s)	0.067	0.044	0.002	2.152	1.395	0.089	96.846	97.753
Steering motor angle error (rad)	0.596	0.373	0.003	19.531	12.295	0.955	96.966	99.686
Steering motor rate error (rad/s)	1.133	0.745	0.027	36.507	23.661	1.516	96.851	98.219
Motor current error (A)	2.326	1.084	0.764	5.891	3.038	2.589	64.319	70.491
v_3 = 90 km/h	FBSC			BSC			Improvement (%)	
	Max	RMS	Mean	Max	RMS	Mean	RMS	Mean
Steering column angle error (rad)	0.031	0.019	≈ 0	0.983	0.631	0.039	96.989	100.000
Steering column rate error (rad/s)	0.060	0.039	0.001	1.957	1.226	0.054	96.819	98.148
Steering motor angle error (rad)	0.519	0.326	0.003	16.691	10.710	0.657	96.956	99.543
Steering motor rate error (rad/s)	1.017	0.663	0.009	33.185	20.793	0.915	96.811	99.016
Motor current error (A)	2.310	1.078	0.764	5.337	2.688	0.579	59.896	-31.952

performance. Systematic errors are greatly eliminated once the BSC algorithm is replaced with the FBSC. The results obtained in the second case are listed in Table 4.

Some comments are made based on the simulation results, as follows:

+ Assisted torque increases or decreases linearly according to driver torque in a stable working range. When the value of driver torque reaches maximum ($T_d = T_{d\_max}$), assisted torque will reach saturation ($T_a = T_{a\_max}$).

+ The output values decrease sharply as the velocity increases. This is caused by a decrease in assisted torque and an increase in road reaction torque.

+ Concerning the sine wave steering type (1st case), the output signals received from the BSC controller are phase

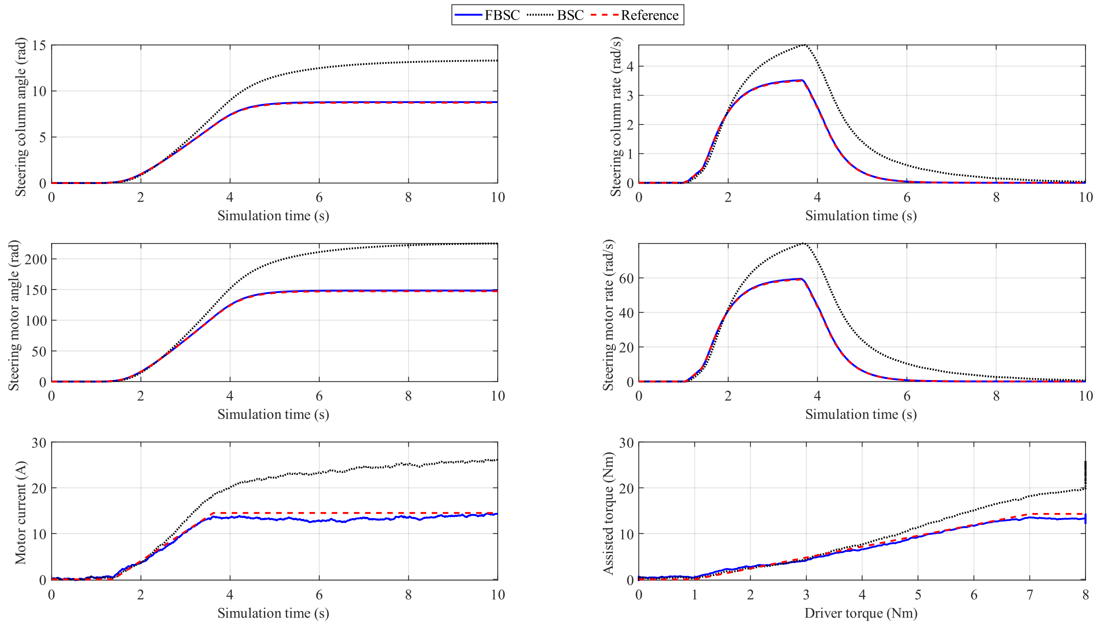

FIGURE 11. **Simulation results (v_1, J-turn steering).**

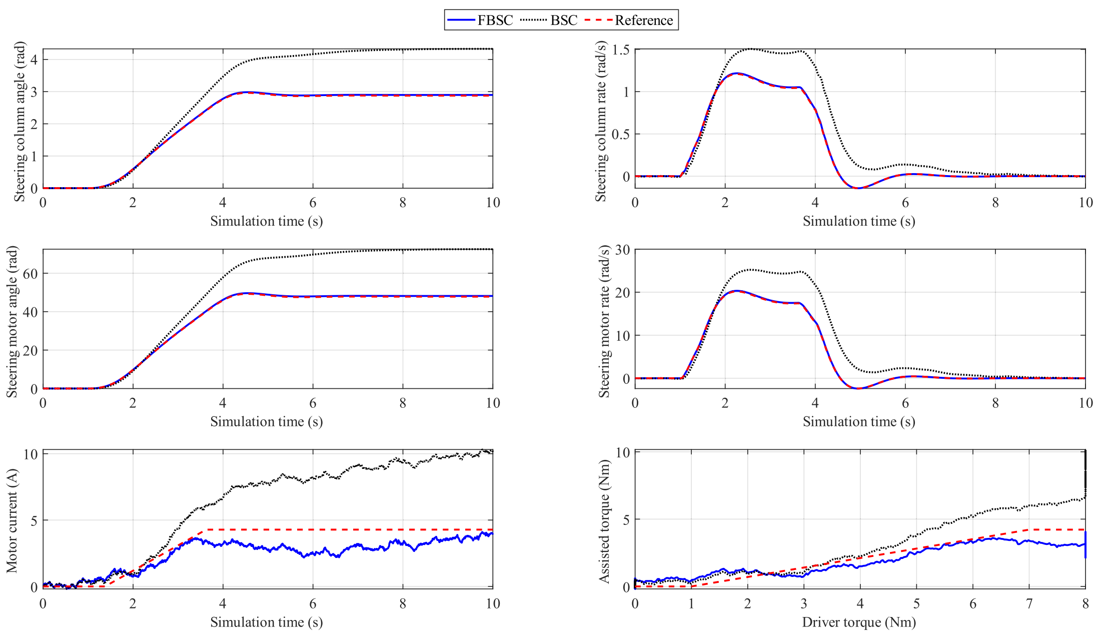

FIGURE 12. **Simulation results (v_2, J-turn steering).**

delayed with average error. Regarding the J-turn steering type (2nd case), the system error is substantial when this technique controls the EPS system.

+ Once the conventional backstepping controller is replaced by fuzzy backstepping, the phase shift phenomenon is almost completely eliminated, and the system error is reduced to extremely small. This conclusion is proper in many investigated conditions, even when driver torque and vehicle speed vary.

Compared with some previous publications, the algorithm proposed in this work provides superior performance. Firstly, the motor current obtained from the FBSC algorithm is lower than that of PID-ACO [10]. This shows that the power consumption of the proposed controller has been improved. Secondly, the phase delay phenomenon is eliminated when steering at low speed, while this problem still exists when applying the BPNN PID technique [12]. Thirdly, the chattering phenomenon is significantly eliminated when applying

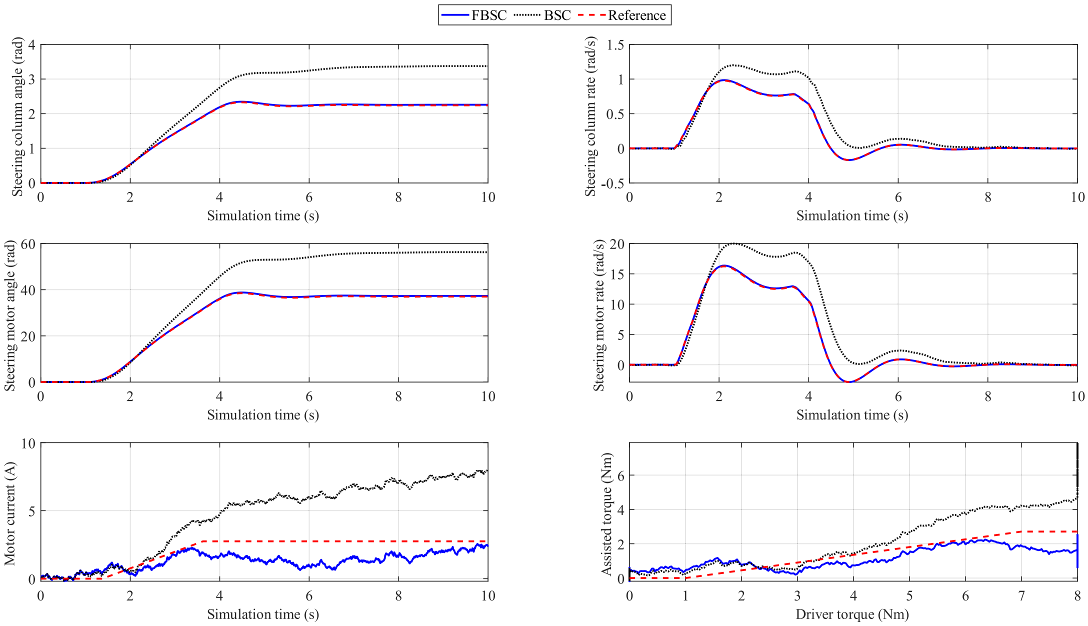

FIGURE 13. Simulation results (v_3, J-turn steering).

TABLE 4. Simulation results (2nd case).

v_1 = 20 km/h	FBSC			BSC			Improvement (%)	
	Max	RMS	Mean	Max	RMS	Mean	RMS	Mean
Steering column angle error (rad)	0.065	0.041	0.027	4.578	2.505	1.609	98.363	98.322
Steering column rate error (rad/s)	0.036	0.010	0.004	1.598	0.557	0.301	98.205	98.671
Steering motor angle error (rad)	1.103	0.693	0.464	77.828	42.589	27.356	98.373	98.304
Steering motor rate error (rad/s)	0.604	0.176	0.070	26.907	9.469	5.122	98.141	98.633
Motor current error (A)	2.031	0.835	0.415	11.681	6.170	4.179	86.467	90.069
v_2 = 70 km/h	FBSC			BSC			Improvement (%)	
	Max	RMS	Mean	Max	RMS	Mean	RMS	Mean
Steering column angle error (rad)	0.022	0.015	0.011	1.454	0.881	0.610	98.297	98.197
Steering column rate error (rad/s)	0.014	0.004	0.002	0.563	0.213	0.118	98.122	98.305
Steering motor angle error (rad)	0.380	0.249	0.181	24.709	14.981	10.371	98.338	98.255
Steering motor rate error (rad/s)	0.199	0.076	0.034	9.411	3.618	2.001	97.899	98.301
Motor current error (A)	2.106	0.889	0.516	6.035	3.084	2.212	71.174	76.673
v_3 = 90 km/h	FBSC			BSC			Improvement (%)	
	Max	RMS	Mean	Max	RMS	Mean	RMS	Mean
Steering column angle error (rad)	0.018	0.012	0.009	1.132	0.745	0.553	98.389	98.373
Steering column rate error (rad/s)	0.012	0.003	0.001	0.446	0.166	0.092	98.193	98.913
Steering motor angle error (rad)	0.305	0.212	0.163	19.247	12.665	9.397	98.326	98.265
Steering motor rate error (rad/s)	0.165	0.058	0.024	7.451	2.814	1.570	97.939	98.471
Motor current error (A)	2.116	0.961	0.610	5.254	2.802	2.124	65.703	71.281

the proposed control technique, compared with [15], [24], [25], [27], and [29]. Finally, systematic errors are eliminated almost completely, which provides higher efficiency than [17].

IV. CONCLUSION

The robust fuzzy backstepping control algorithm is established in this paper to control the performance of the EPS system. The simulation is performed with two cases corresponding to two steering types. The research shows that the output signals tend to closely follow the reference signal with almost no error if and only if the FBSC technique controls the EPS system, as this paper suggests. In addition, phase lag is almost completely eliminated, and energy consumption is maintained within acceptable tolerances. System stability is ensured under investigated conditions, even when driver torque and vehicle speed change.

Although the proposed algorithm (FBSC) offers superior advantages over the conventional BSC algorithm, some drawbacks still exist: 1) The systematic error must still be eliminated to zero; 2) The motor current signal fluctuates due to disturbances. These issues will be resolved in the following papers.

V. FUTURE WORK

In the future, some experiments can be done to evaluate the quality of the proposed controller. These experiments can be performed based on some of the following settings:

+ Prepare a model of the steering system equipped with EPS installed on the test bench. The sensors must be installed in appropriate locations (steering wheel, steering motor, vehicle speed sensors, and others).

+ The proposed control algorithm is updated to a MicroAutobox II, a real-time device that can work without user intervention through auto-code generation.

+ Perform steering at different speeds (described in the simulation). Then, measure the sensor's output values and compare them to the simulation results.

Some challenges of conducting real-time experiments include the following: Firstly, the difference between the experimental system's technical parameter values and the simulation's parameters. Secondly, the influence of sensor noise during measurement. Thirdly, there is instability in control signals and power grid systems. Fourthly, the problems are related to a DC motor fault.

The first problem can be solved by carefully measuring the technical parameters. Then, the simulation will be rerun according to the actual values. The use of filters is an effective solution to reject sensor noise. Some other methods to solve the second issue can be found in [48], and [49]. The third issue can be addressed by applying a multisegmented intelligent solution introduced in [50]. Some effective methods to solve the last problem should be referred to [51] and [52].

REFERENCES

[1] L. Xia and H. Jiang, "An electronically controlled hydraulic power steering system for heavy vehicles," *Adv. Mech. Eng.*, vol. 8, no. 11, Nov. 2016, Art. no. 168781401667956, doi: 10.1177/1687814016679566.

[2] M. B. Baharom, K. Hussain, and A. J. Day, "Design of full electric power steering with enhanced performance over that of hydraulic power-assisted steering," *Proc. Inst. Mech. Eng. D, J. Automobile Eng.*, vol. 227, no. 3, pp. 390–399, Jan. 2013, doi: 10.1177/0954407012468413.

[3] A. Amirkhani, M. Shirzadeh, and J. Heydari, "Automotive electric power steering control with robust observer based neuroadaptive type-2 radial basis function methodology," *IEEE Open J. Veh. Technol.*, vol. 5, pp. 592–605, 2024, doi: 10.1109/OJVT.2024.3383516.

[4] D. Ramasamy, "An approach for steering wheel angle evaluation without using a true power-on steering angle sensor in electric power steering systems," *J. Inst. Eng. India B*, vol. 104, no. 3, pp. 563–568, Apr. 2023, doi: 10.1007/s40031-023-00884-1.

[5] R. Hartono, H. R. Cha, and K. J. Shin, "Design of electric power steering system identification and control for autonomous vehicles based on artificial neural network," *IEEE Access*, 2024, doi: 10.1109/ACCESS.2024.3387460.

[6] Z. Wang and H. R. Karimi, "Experimental study on antivibration control of electrical power steering systems," *J. Appl. Math.*, vol. 2014, pp. 1–7, Jan. 2014, doi: 10.1155/2014/450427.

[7] A. Khalkhali, M. H. Shojaeefard, M. Dahmardeh, and H. Sotoudeh, "Optimal design and applicability of electric power steering system for automotive platform," *J. Central South Univ.*, vol. 26, no. 4, pp. 839–851, Apr. 2019, doi: 10.1007/s11771-019-4053-3.

[8] Z. Fu, Y. Lu, D. Zhao, P. Yuan, and Y. Guo, "A novel dual power-driven electric power steering system for electric commercial vehicles," *Adv. Mech. Eng.*, vol. 15, no. 9, Sep. 2023, Art. no. 16878132231200314, doi: 10.1177/16878132231200314.

[9] M. K. Hassan, N. A. M. Azubir, H. M. I. Nizam, S. F. Toha, and B. S. K. K. Ibrahim, "Optimal design of electric power assisted steering system (EPAS) using GA-PID method," *Proc. Eng.*, vol. 41, pp. 614–621, Jan. 2012, doi: 10.1016/j.proeng.2012.07.220.

[10] R. A. Hanifah, S. F. Toha, S. Ahmad, and M. K. Hassan, "Swarm-intelligence tuned current reduction for power-assisted steering control in electric vehicles," *IEEE Trans. Ind. Electron.*, vol. 65, no. 9, pp. 7202–7210, Sep. 2018, doi: 10.1109/TIE.2017.2784344.

[11] Z. Cao and S. Zheng, "MR-SAS and electric power steering variable universe fuzzy PID integrated control," *Neural Comput. Appl.*, vol. 31, no. 4, pp. 1249–1258, Jul. 2017, doi: 10.1007/s00521-017-3157-7.

[12] Y. Li, G. Wu, L. Wu, and S. Chen, "Electric power steering nonlinear problem based on proportional–integral–derivative parameter self-tuning of back propagation neural network," *Proc. Inst. Mech. Eng. C, J. Mech. Eng. Sci.*, vol. 234, no. 23, pp. 4725–4736, May 2020, doi: 10.1177/0954406220926549.

[13] Z. Zheng and J. Wei, "Research on electric power steering fuzzy PI control strategy based on phase compensation," *Int. J. Dyn. Control*, vol. 11, no. 4, pp. 1867–1879, Nov. 2022, doi: 10.1007/s40435-022-01077-2.

[14] A. Diab, G. Valmorbida, and W. Pasillas-Lépine, "Linear assistance filter design for electric power steering systems with improved delay margin," *Int. J. Control*, vol. 97, no. 5, pp. 1118–1135, Apr. 2023, doi: 10.1080/00207179.2023.2201648.

[15] W. Kim, Y. S. Son, and C. C. Chung, "Torque-overlay-based robust steering wheel angle control of electrical power steering for a lane-keeping system of automated vehicles," *IEEE Trans. Veh. Technol.*, vol. 65, no. 6, pp. 4379–4392, Jun. 2016, doi: 10.1109/TVT.2015.2473115.

[16] R. Manca, S. Circosta, I. Khan, S. Feraco, S. Luciani, N. Amati, A. Bonfitto, and R. Galluzzi, "Performance assessment of an electric power steering system for driverless formula student vehicles," *Actuators*, vol. 10, no. 7, p. 165, Jul. 2021, doi: 10.3390/act10070165.

[17] J. C. Ramos-Fernández, V. López-Morales, M. A. Márquez-Vera, J. M. X. Pérez, and J. Suarez-Cansino, "Neuro-fuzzy modelling and stable PD controller for angular position in steering systems," *Int. J. Automot. Technol.*, vol. 22, no. 6, pp. 1495–1503, Nov. 2021, doi: 10.1007/s12239-021-0129-9.

[18] C. Chitu, J. Lackner, M. Horn, P. Srikanth Pullagura, H. Waser, and M. Kohlböck, "Controller design for an electric power steering system based on LQR techniques," *COMPEL, Int. J. Comput. Math. Electr. Electron. Eng.*, vol. 32, no. 3, pp. 763–775, May 2013, doi: 10.1108/03321641311305737.

[19] M. Irmer and H. Henrichfreise, "Design of a robust LQG compensator for an electric power steering," *IFAC-PapersOnLine*, vol. 53, no. 2, pp. 6624–6630, Jan. 2020, doi: 10.1016/j.ifacol.2020.12.082.

[20] K. Yamamoto, O. Sename, D. Koenig, and P. Moulaire, "Design and experimentation of an LPV extended state feedback control on electric power steering systems," *Control Eng. Pract.*, vol. 90, pp. 123–132, Sep. 2019, doi: 10.1016/j.conengprac.2019.06.004.

[21] D. Lee, K.-S. Kim, and S. Kim, "Controller design of an electric power steering system," *IEEE Trans. Control Syst. Technol.*, vol. 26, no. 2, pp. 748–755, Mar. 2018, doi: 10.1109/TCST.2017.2679062.

[22] W.-Z. Zhao, Y.-J. Li, C.-Y. Wang, T. Zhao, and X.-Y. Gu, "H∞ control of novel active steering integrated with electric power steering function," *J. Central South Univ.*, vol. 20, no. 8, pp. 2151–2157, Jul. 2013, doi: 10.1007/s11771-013-1719-0.

[23] C. Dannöhl, S. Müller, and H. Ulbrich, "H∞-control of a rack-assisted electric power steering system," *Vehicle Syst. Dyn.*, vol. 50, no. 4, pp. 527–544, Apr. 2012, doi: 10.1080/00423114.2011.603051.

[24] L. Khasawneh and M. Das, "A robust electric power-steering-angle controller for autonomous vehicles with disturbance rejection," *Electronics*, vol. 11, no. 9, p. 1337, Apr. 2022, doi: 10.3390/electronics11091337.

[25] D. Lee, K. Yi, S. Chang, B. Lee, and B. Jang, "Robust steering-assist torque control of electric-power-assisted-steering systems for target steering wheel torque tracking," *Mechatronics*, vol. 49, pp. 157–167, Feb. 2018, doi: 10.1016/j.mechatronics.2017.12.007.

[26] S. Lu, M. Lian, M. Liu, C. Cho, and C. Piao, "Adaptive fuzzy sliding mode control for electric power steering system," *J. Mech. Sci. Technol.*, vol. 31, no. 6, pp. 2643–2650, Jun. 2017, doi: 10.1007/s12206-017-0507-4.

[27] S. Na, Z. Li, F. Qiu, and C. Zhang, "Torque control of electric power steering systems based on improved active disturbance rejection control," *Math. Problems Eng.*, vol. 2020, pp. 1–13, Apr. 2020, doi: 10.1155/2020/6509607.

[28] X. Ma, Y. Guo, and L. Chen, "Active disturbance rejection control for electric power steering system with assist motor variable mode," *J. Franklin Inst.*, vol. 355, no. 3, pp. 1139–1155, Feb. 2018, doi: 10.1016/j.jfranklin.2017.12.024.

[29] Z. Zheng and J. Wei, "Research on active disturbance rejection control strategy of electric power steering system under extreme working conditions," *Meas. Control*, vol. 57, no. 1, pp. 90–100, Aug. 2023, doi: 10.1177/00202940231192986.

[30] D. Fu, D.-Z. Li, and W.-B. Shangguan, "Model-based feedforward control for suppressing torque oscillation of electric power steering system," *Proc. Inst. Mech. Eng. D, J. Automobile Eng.*, vol. 236, nos. 10–11, pp. 2306–2317, Nov. 2021, doi: 10.1177/09544070211058347.

[31] D. Lee, B. Jang, M. Han, and K.-S. Kim, "A new controller design method for an electric power steering system based on a target steering torque feedback controller," *Control Eng. Pract.*, vol. 106, Jan. 2021, Art. no. 104658, doi: 10.1016/j.conengprac.2020.104658.

[32] G. Shi, M. Song, C. Ju, S. Wang, and P. Qiao, "Adaptive robust steering strategy for electro-hydraulic hybrid steering system based on backstepping method," *Proc. Inst. Mech. Eng. D, J. Automobile Eng.*, Jun. 2023, Art. no. 095440702311790, doi: 10.1177/09544070231179073.

[33] D. N. Nguyen and T. A. Nguyen, "Proposing a BSPID control strategy considering external disturbances for electric power steering (EPS) systems," *IEEE Access*, vol. 11, pp. 143230–143249, 2023, doi: 10.1109/ACCESS.2023.3343914.

[34] T. A. Nguyen, "Development of a novel integrated control strategy for automotive electric power steering systems," *IEEE Trans. Autom. Sci. Eng.*, Jan. 2024, doi: 10.1109/TASE.2024.3356509.

[35] X. Li, X.-P. Zhao, and J. Chen, "Controller design for electric power steering system using T-S fuzzy model approach," *Int. J. Autom. Comput.*, vol. 6, no. 2, pp. 198–203, Apr. 2009, doi: 10.1007/s11633-009-0198-0.

[36] Y.-C. Hung, F.-J. Lin, J.-C. Hwang, J.-K. Chang, and K.-C. Ruan, "Wavelet fuzzy neural network with asymmetric membership function controller for electric power steering system via improved differential evolution," *IEEE Trans. Power Electron.*, vol. 30, no. 4, pp. 2350–2362, Apr. 2015, doi: 10.1109/TPEL.2014.2327693.

[37] D. Fu, S. Rakheja, W.-B. Shangguan, and H. Yin, "Robust control for fuzzy electric power steering system: A two-layer performance approach," *J. Vib. Control*, vol. 28, nos. 5–6, pp. 536–550, Mar. 2021, doi: 10.1177/10775463211003420.

[38] S. You, G. Kim, S. Lee, D. Shin, and W. Kim, "Neural approximation-based adaptive control using reinforced gain for steering wheel torque tracking of electric power steering system," *IEEE Trans. Syst., Man, Cybern., Syst.*, vol. 53, no. 7, pp. 4216–4225, Jul. 2023, doi: 10.1109/TSMC.2023.3241452.

[39] T. Yang, N. Sun, and Y. Fang, "Neuroadaptive control for complicated underactuated systems with simultaneous output and velocity constraints exerted on both actuated and unactuated states," *IEEE Trans. Neural Netw. Learn. Syst.*, vol. 34, no. 8, pp. 4488–4498, Aug. 2023, doi: 10.1109/TNNLS.2021.3115960.

[40] T. Yang, N. Sun, H. Chen, and Y. Fang, "Adaptive optimal motion control of uncertain underactuated mechatronic systems with actuator constraints," *IEEE/ASME Trans. Mechatronics*, vol. 28, no. 1, pp. 210–222, Feb. 2023, doi: 10.1109/TMECH.2022.3192002.

[41] J. Rahulkumar and R. Narayanamoorthi, "Power control and efficiency enhancement topology for dual receiver wireless power transfer EV quasi-dynamic charging," in *Proc. IEEE Int. Transp. Electrific. Conf. (ITEC-India)*, Chennai, India, Dec. 2023, pp. 1–6, doi: 10.1109/ITEC-India59098.2023.10471417.

[42] K. Prasanna, D. Kirubakaran, J. Rahulkumar, and J. A. Rudhran, "Implementation of positive output super lift Luo converter for photo voltaic system," *Int. Res. J. Eng. Technol.*, vol. 2, no. 3, pp. 447–452, 2015.

[43] R. R. Sorial, M. H. Soliman, H. M. Hasanien, and H. E. A. Talaat, "A vector controlled drive system for electrically power assisted steering using Hall-effect sensors," *IEEE Access*, vol. 9, pp. 116485–116499, 2021, doi: 10.1109/ACCESS.2021.3105609.

[44] J. I. Park, K. Jeon, and K. Yi, "An investigation on the energy-saving effect of a hybrid electric-power steering system for commercial vehicles," *Proc. Inst. Mech. Eng. D, J. Automobile Eng.*, vol. 233, no. 6, pp. 1623–1648, Jun. 2018, doi: 10.1177/0954407018777579.

[45] A. Murilo, R. Rodrigues, E. L. S. Teixeira, and M. M. D. Santos, "Design of a parameterized model predictive control for electric power assisted steering," *Control Eng. Pract.*, vol. 90, pp. 331–341, Sep. 2019, doi: 10.1016/j.conengprac.2019.07.010.

[46] B. Jang, D. Lee, K. Kim, and K.-S. Kim, "Road torque modeling for electric power steering systems," *Int. J. Automot. Technol.*, vol. 23, no. 3, pp. 765–773, Jun. 2022, doi: 10.1007/s12239-022-0068-0.

[47] T. A. Nguyen, "Establishing a novel adaptive fuzzy control algorithm for an active stabilizer bar with complex automotive dynamics model," *Ain Shams Eng. J.*, vol. 15, no. 1, Jan. 2024, Art. no. 102334, doi: 10.1016/j.asej.2023.102334.

[48] Z. Ning, Y. Mao, Y. Huang, Z. Xi, and C. Zhang, "A measurement noise rejection method in the feedback control system based on noise observer," *IEEE Sensors J.*, vol. 21, no. 2, pp. 1686–1693, Jan. 2021, doi: 10.1109/JSEN.2020.3015837.

[49] O. Babayomi, Z. Zhang, Z. Li, M. L. Heldwein, and J. Rodriguez, "Robust predictive control of grid-connected converters: Sensor noise suppression with parallel-cascade extended state observer," *IEEE Trans. Ind. Electron.*, vol. 71, no. 4, pp. 3728–3740, Apr. 2024, doi: 10.1109/TIE.2023.3279565.

[50] M. Z. Yousaf, S. Mirsaeidi, S. Khalid, A. Raza, C. Zhichu, W. U. Rehman, and F. Badshah, "Multisegmented intelligent solution for MT-HVDC grid protection," *Electronics*, vol. 12, no. 8, p. 1766, Apr. 2023, doi: 10.3390/electronics12081766.

[51] M. Z. Yousaf, S. Khalid, M. F. Tahir, A. Tzes, and A. Raza, "A novel DC fault protection scheme based on intelligent network for meshed DC grids," *Int. J. Electr. Power Energy Syst.*, vol. 154, Dec. 2023, Art. no. 109423, doi: 10.1016/j.ijepes.2023.109423.

[52] M. Z. Yousaf, H. Liu, A. Raza, and A. Mustafa, "Deep learning-based robust DC fault protection scheme for meshed HVDC grids," *CSEE J. Power Energy Syst.*, vol. 9, no. 6, pp. 2423–2434, Nov. 2023, doi: 10.17775/CSEEJPES.2021.03550.

DUC NGOC NGUYEN received the Ph.D. degree in automotive engineering from Chongqing University, in 2011. He is currently working as an Associate Professor with Thuyloi University, Hanoi, Vietnam. He is also the Head of the Department of Automotive Engineering. He has published many international articles relating to vehicle dynamics and control.

TUAN ANH NGUYEN was born in Hanoi, Vietnam, in 1995. He received the master's degree from Hanoi University of Science and Technology (HUST), in 2019. He is currently a Lecturer with the Department of Automotive Engineering, Thuyloi University, Hanoi. He has published several international articles. His research interests include automotive engineering, vehicle dynamics, and optimization and control.